

基于壁面反射增强模型的熔石英刻蚀形貌形成机理研究

陈军^{1,2}, 王林^{1*}, 魏朝阳¹, 邵建达¹

¹中国科学院上海光学精密机械研究所精密光学制造与检测中心, 上海 201800;

²中国科学院大学材料科学与光电技术学院, 北京 100049

摘要 大气等离子体刻蚀是一种非接触式、材料去除可控的加工方法,在光学元件的高精度加工中具有广泛的应用前景。但是大气等离子体刻蚀后元件存在表面形貌恶化的问题,严重影响元件的性能和使用寿命。进行氢氟酸刻蚀实验,证明了元件表面形貌的恶化是由氟碳化合物和表面凹坑微结构两个原因引起的。为了解释表面凹坑微结构的形成,提出基于 micro-mask 壁面反射增强理论的凹坑形成模型,并开展了样品表面旋涂金纳米颗粒充当 micro-mask 的刻蚀实验。实验结果验证了 micro-mask 壁面反射增强模型的正确性,为解决大气等离子体刻蚀后元件表面形貌恶化问题提供了新的思路和方法。

关键词 壁面反射增强; 熔石英; 表面形貌; 形成机理; 大气等离子体

中图分类号 O436 **文献标志码** A

DOI: 10.3788/AOS230841

1 引言

熔石英元件具有优秀的机械和光学性能,在激光聚变、空间探测等领域获得广泛的应用^[1-3]。大气等离子体刻蚀是一种基于纯化学反应去除材料的加工方式,具有成本低、非接触、材料去除可控和不引入亚表面损伤的特点^[4-5],在熔石英元件的高精度、低缺陷加工中具有巨大的应用潜力^[6-8]。然而,纯化学反应的材料去除机理导致大气等离子体刻蚀后熔石英元件表面形貌恶化^[9-11],严重影响了元件的性能和使用寿命^[12-13]。因此,揭示大气等离子体刻蚀过程中元件表面形貌恶化机理日益迫切。

大气等离子体刻蚀后熔石英元件表面形貌恶化主要是由沉积物和凹坑结构两种原因引起的。Jin 等^[14-15]认为大气等离子体刻蚀过程中沉积的氟碳化合物薄膜是引起表面形貌恶化的最主要原因,并提出在反应气体中添加 O₂ 来抑制氟碳化合物的沉积。Jiang 等^[16]认为抑制剂粒子和基底的结合能不匹配,导致抑制剂粒子优先相互结合形成的大颗粒沉积在元件表面,导致表面形貌恶化。Jung 等^[17]提出了等离子体诱导坑点损伤(plasma induced pitting damage)的概念,认为等离子体的不均匀轰击导致元件表面出现凹坑结构。Choi 等^[18]认为样品表面存在的金属异物对反应产物具有催化作用,诱导颗粒物沉积,由

于颗粒物的反射作用引起周围离子束增强,在元件表面会形成凹坑^[19-20],但该理论仅局限于概念性阐述。Li 等^[21]的研究中,大气等离子体在熔石英表面进行长时间驻留,熔石英表面出现“圆环”图案,该图案中透明区域和不透明区域含有相同种类的化学元素且比例相近,两个区域的凹坑尺寸和数量完全不同,但未进一步分析和验证表面凹坑的形成机理。现有文献主要集中在沉积物和凹坑结构引起的表面形貌恶化现象本身和对现象的定性解释,缺乏对凹坑形成机理的深入研究和实验验证。因此,深刻理解等离子体刻蚀后表面形貌的形成机理,对优化等离子体刻蚀在光学制造链中的作用和提升光学元件的加工质量至关重要。

本文研究了大气等离子体刻蚀抛光石英的表面形貌形成机理。通过氢氟酸刻蚀和 X 射线光电子能谱仪(XPS)测量,证明大气等离子体刻蚀后的熔石英元件表面不仅沉积有氟碳化合物,还存在凹坑微结构。然后提出了基于 micro-mask 的壁面反射增强模型,开展了以旋涂金纳米颗粒作为 micro-mask 的刻蚀验证实验,验证了 micro-mask 壁面反射增强模型的正确性。研究成果有利于揭示大气等离子体刻蚀后抛光石英表面形貌的恶化机理,为解释大气等离子体刻蚀导致的抛光石英表面形貌恶化提供依据。

收稿日期: 2023-04-18; 修回日期: 2023-05-19; 录用日期: 2023-05-31; 网络首发日期: 2023-06-28

通信作者: *wanglin@siom.ac.cn

2 装置及实验

2.1 大气等离子体装置

大气等离子体刻蚀去除材料的基本原理是:在射频电源的激励作用下,反应气体电离激发出活性刻蚀粒子,其与元件发生反应,反应产物为气体,逃离元件表面,从而实现材料去除^[22]。大气等离子体刻蚀去除材料的基本化学反应方程为



图 1 为采用的电容耦合大气等离子体装置示意图,其中铝电极为正电极,底座为负电极,待加工元件为阻挡介质。为了避免活性粒子对铝电极的反应腐蚀,铝电极表面涂覆一层氧化铝陶瓷薄膜。大气等离子体激发所使用的载气、反应气体和辅助气体分别是氦气、四氟化碳和氧气^[23]。射频电源的工作频率为 13.56 MHz。

2.2 实验处理

2.2.1 样品准备

所使用的样品是中国建筑材料科学研究总院提供的 JGS1 熔石英玻璃,直径为 50 mm,厚度为 5 mm。所有样品使用传统的氧化铈抛光,并使用氢氟酸进行深刻蚀处理以去除再沉积层和亚表面损伤。在进行刻蚀实验前,采用多频超声去离子水对样品进行清洗并风干,清洗频率依次为 40, 75, 120 kHz,每个频率的清洗时间为 3 min,清洗温度为 45 °C。

2.2.2 大气等离子体刻蚀处理

大气等离子体沿光栅路径对样品进行匀速扫描,光栅路径的点间距和行间距均为 1 mm,扫描速度为 60 mm/min,刻蚀区域是半径为 20 mm 的半圆形区域。为了便于表述和理解,将扫描速度转换为单位长度的

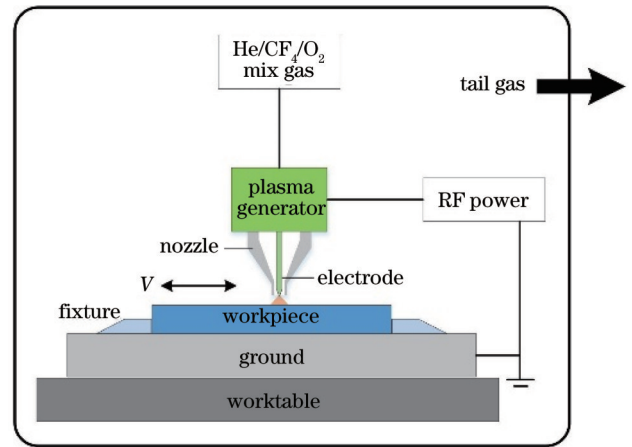


图 1 大气离子体装置示意图

Fig. 1 Schematic of the atmospheric plasma machine

驻留时间,则该扫描速度下对应的驻留时间为 1 s。大气等离子体的刻蚀参数如表 1 所示。

表 1 大气等离子体的刻蚀参数

Table 1 Parameters of plasma etching processing

Driver power	Gas flow rate of He	Gas flow rate of CF ₄	Gas flow rate of O ₂
170 W	1800 mL/min	100 mL/min	20 mL/min

2.2.3 氢氟酸刻蚀处理

对大气等离子体刻蚀后的熔石英样品再进行氢氟酸刻蚀处理。图 2 为大气等离子体刻蚀和氢氟酸刻蚀样品的示意图。将大气等离子体刻蚀后的熔石英样品旋转 90°,再将该样品浸入质量分数为 20% 的氢氟酸中进行均匀刻蚀,采用频率为 1 MHz 的兆声辅助氢氟酸刻蚀,刻蚀时间为 30 min,样品表面的材料去除深度约 5 μm。

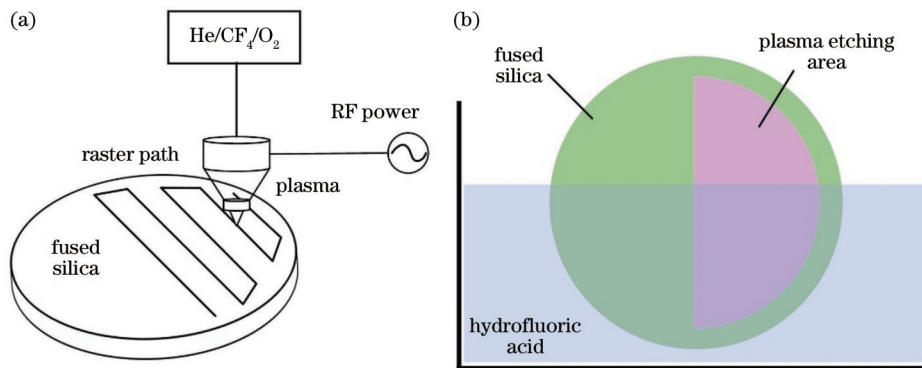


图 2 样品刻蚀处理示意图。(a)大气等离子体刻蚀;(b)氢氟酸刻蚀

Fig. 2 Schematic of sample etching. (a) Plasma etching; (b) hydrofluoric acid etching

2.2.4 表征和测量

使用扫描电子显微镜(AURIGA CrossBeam, Zeiss 公司)观察样品表面的微观形貌。使用 X 射线光电子能谱仪(Scientific K-Alpha, Thermo 公司)测量大气等离子体和氢氟酸刻蚀后样品表面的化学元素组

成。使用原子力显微镜(Veeco Dimension 3100)观察大气等离子体刻蚀后样品表面凹坑的尺寸信息。使用白光轮廓仪(NewView 7200, Zygo 公司)观察大气等离子体刻蚀后样品的表面形貌和粗糙度。

3 实验结果

3.1 大气等离子体刻蚀后再经氢氟酸刻蚀的表面形貌

为了分析元件表面形貌恶化的原因,对大气等离子体刻蚀后熔石英样品进行氢氟酸刻蚀。首先使用 2.2.2 节参数下的大气等离子体对样品进行均匀刻蚀,再使用 2.2.3 节参数下的氢氟酸对样品进行刻

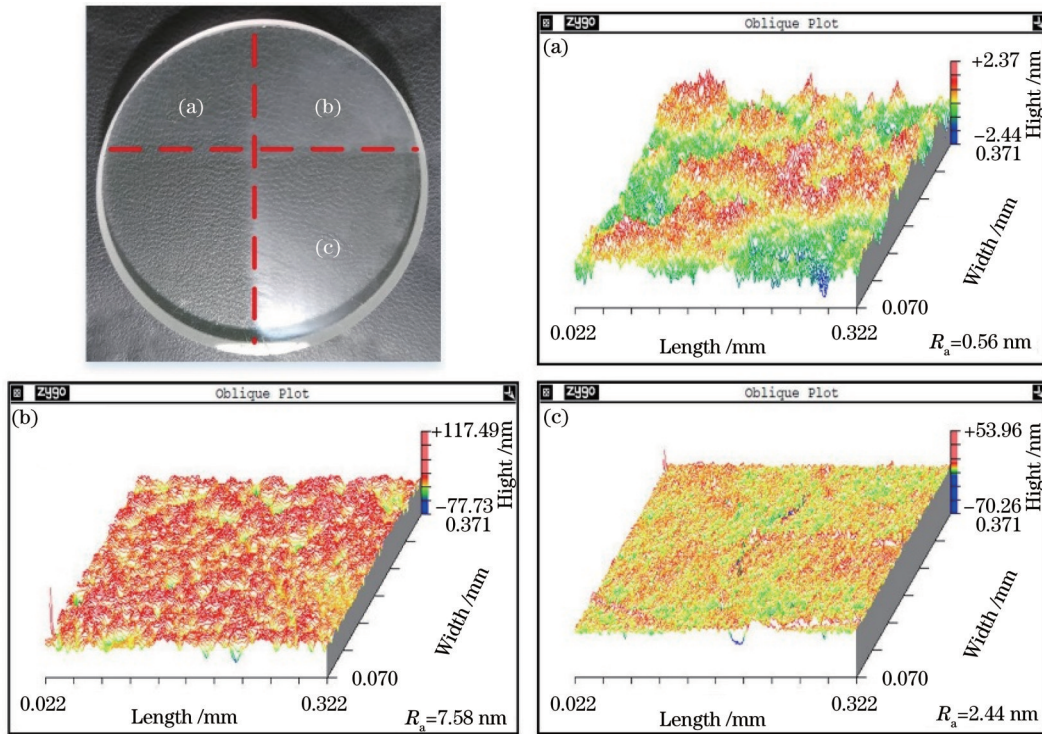


图 3 大气等离子体和氢氟酸刻蚀后样品外观及三维形貌

Fig. 3 Surface morphology of sample etched by plasma and then hydrofluoric acid

图 3 的测试结果表明:相比未处理的样品表面(粗糙度 $R_a=0.56$ nm),大气等离子体刻蚀后,样品表面形貌非常粗糙,粗糙度 $R_a=7.58$ nm;经过氢氟酸刻蚀后,样品表面变得相对平坦,粗糙度 $R_a=2.44$ nm。由图 4 可以看出,经大气等离子体刻蚀后的熔石英样品表面元素组成由 Si、O、C 变为 Si、O、C 和 F,样品表面出现了氟元素。其中 Si 和 O 是熔石英材料本身的组成元素,C 和 F 可能来自大气等离子体刻蚀中反应气体中电离或活性粒子与样品表面的反应产物。根据图 5 中 C 元素谱线峰值对应的结合能,大气等离子体刻蚀后的样品表面 C1s 元素谱线出现两个峰值,结合能峰值分别位于 284.6 eV 和 286.5 eV 处。对照标准谱可知,在 C1s 峰值处 C 元素以 C—C 和 C—CF_n 的形式存在。在 284.6 eV 处的 C—C 通常认为是样品暴露在空气中引入的污染导致的,在 286.5 eV 处的 C—CF_n 则源自大气等离子体刻蚀反应中的产物,即氟碳化合物^[14]。经过氢氟酸刻蚀后,样品表面的氟元素稍有减少。

蚀。图 3 为大气等离子体和氢氟酸刻蚀后样品外观及三维形貌。图 3(a)为熔石英元件原始表面,图 3(b)为大气等离子体刻蚀的区域,图 3(c)为大气等离子体刻蚀+氢氟酸刻蚀的区域。图 4 为大气等离子体刻蚀后再使用氢氟酸刻蚀的样品表面的元素全谱,左上角的曲线为 binding energy 在 650~720 eV 范围内的放大图。图 5 为大气等离子体刻蚀后样品表面的 C 元素谱。

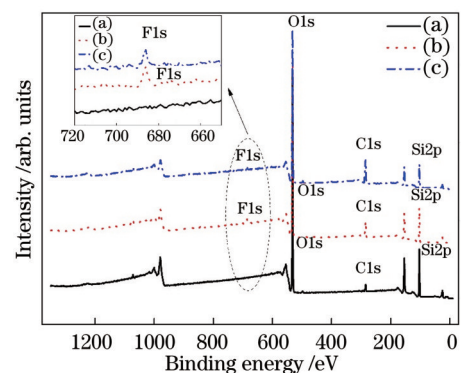


图 4 大气等离子体刻蚀后再使用氢氟酸刻蚀后样品表面的元素全谱

Fig. 4 Full spectra of elements of surface topography of sample etched by plasma and then hydrofluoric acid

图 6 为大气等离子体刻蚀后再使用氢氟酸刻蚀的样品表面的扫描电子显微镜图。可以发现:大气等离子体刻蚀后,样品表面出现了密集分布的小凹坑和较大的轮廓包络,并存在直径约 0.1 μ m 的颗粒;经过氢

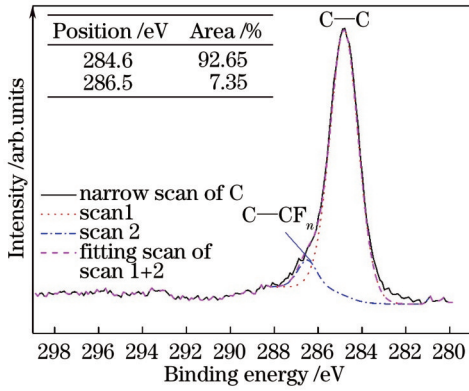


图 5 大气等离子体刻蚀后样品表面的 C 元素谱

Fig. 5 C narrow spectra of surface topography of sample etched by plasma

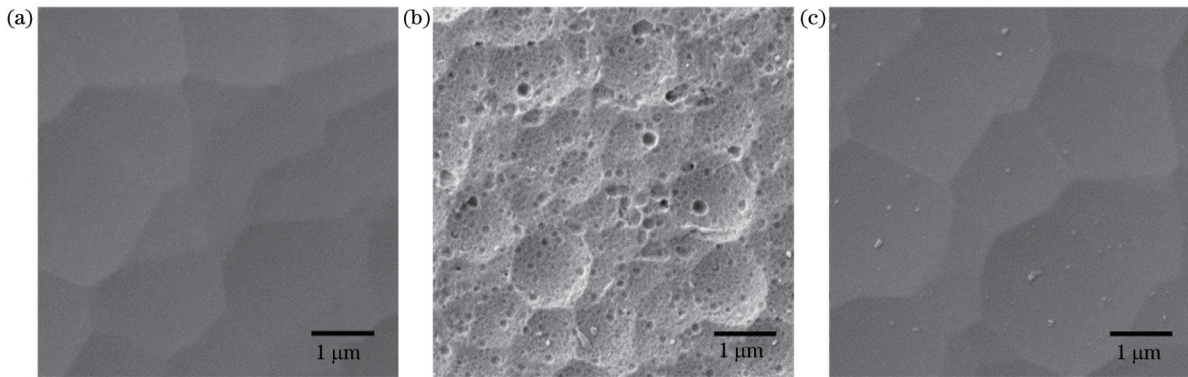
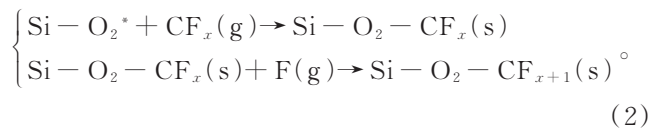


图 6 大气等离子体和氢氟酸刻蚀后样品的扫描电子显微镜图。(a) 刻蚀前样品形貌；(b) 大气等离子体刻蚀后的样品形貌；(c) 氢氟酸刻蚀后的样品形貌

Fig. 6 Scanning electron microscope (SEM) picture of surface topography of sample. (a) Initial surface topography before etching; (b) surface morphology etching by plasma; (c) surface morphology etching by plasma and then hydrofluoric acid

3.2 刻蚀过程中颗粒的形成

为了分析样品表面凹坑的形成机理,使用扫描电子显微镜在 50000 倍下观察凹坑的细节信息,如图 7 所示。发现凹坑的底部存在颗粒沉积物,且颗粒沉积物的周围仍存在微小凹坑,因此推断样品表面凹坑的形成与颗粒沉积物有关。Choi 等^[18]在制备铬掩模板时,最早提出了离子束入射至 mask(金属氯化物)表面时,mask 的壁面反射会引起周围离子束增强,从而在元件表面刻蚀成坑的猜想解释。但是该猜想只是针对 mask,缺少实验验证。本文在 Choi 等研究的基础上,提出了一种基于 micro-mask 的壁面反射增强模型。在大气等离子体刻蚀过程中,刻蚀反应中的氟碳化合物基团(CF_x)会吸附于元件表面形成不挥发的沉积物(氟碳化合物)^[25],同时不挥发的沉积物充当 micro-mask。氟碳化合物基团(CF_x)在 SiO₂ 表面的吸附过程可以表示为



氟酸刻蚀后,表面密集的小凹坑已经消失,但直径约 0.1 μm 的颗粒和大的轮廓包络仍然存在。这是因为,大气等离子体刻蚀反应中电离生成的氟碳化合物基团吸附于样品表面,形成氟碳化合物。在经过氢氟酸刻蚀处理后,样品表面的沉积物得到有效去除,同时表面凹坑也得到扩展合并。氢氟酸具有各向同性刻蚀的特点,其可以刻蚀去掉表面的沉积物,但无法刻蚀去除表面的结构信息。通过组合刻蚀实验,认为经过大气等离子体刻蚀后的样品表面不仅沉积有一层氟碳化合物,同时还存在凹坑微结构。需要说明的是,本文所使用的熔石英样品均为氢氟酸深刻蚀后的样品。氢氟酸深刻蚀可以完全打开和去除抛光石英的再沉积层和亚表面损伤^[24]。因此,观察到的凹坑微结构是伴随着大气等离子体刻蚀反应产生的,而不是由亚表面损伤引起的。

当刻蚀粒子入射至样品表面时,micro-mask 的壁面使刻蚀粒子发生反射增强,导致 micro-mask 周围的刻蚀速率增大,从而在元件表面形成凹坑结构。

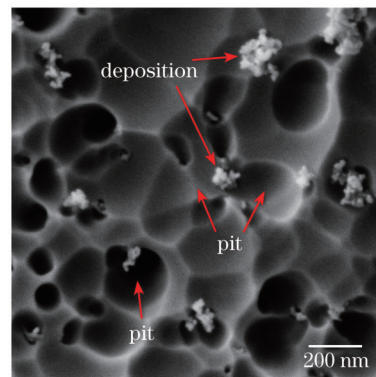


图 7 扫描电子显微镜观察到的在 50000 倍率下熔石英样品的表面形貌

Fig. 7 Surface morphology of fused silica under SEM (50000× magnification)

4 表面凹坑形成机理模型及验证

图 8(a)为 micro-mask 壁面反射增强模型示意图。

假设 micro-mask 为理想的球形颗粒,并且刻蚀粒子垂直入射,其中入射点为 P ,入射点的法线为 OP , θ 为入射点法线方向和水平方向的夹角, H 为 micro-mask 相对元件基准平面的高度, R 为 micro-mask 的半径。考虑到反射粒子需要到达元件表面才会引起刻蚀,因此 θ 角的取值范围为 $0 < \theta < 45^\circ$ 。由几何关系推导,反射

的刻蚀粒子在水平方向上的落点位置 x 可以表示为

$$x = (H + r + r \sin \theta) \tan(2\theta) \quad (3)$$

图 8(b) 为反射刻蚀粒子在水平方向上归一化的粒子数量分布曲线,其中 X 轴表示水平方向上距 micro-mask 中心的距离, Y 轴表示归一化的刻蚀粒子数量。

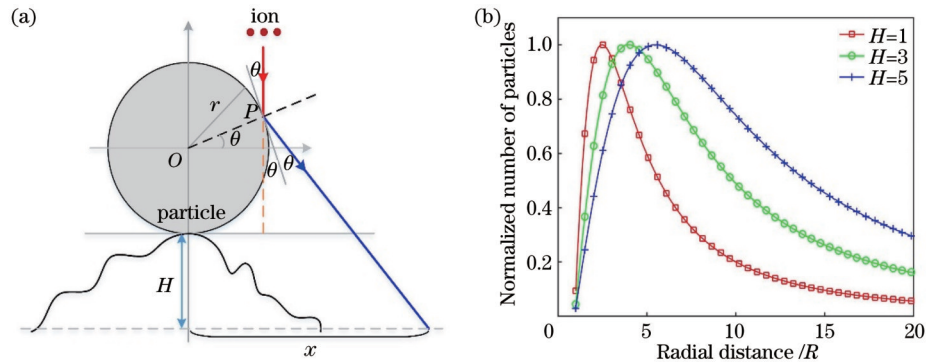


图 8 micro-mask 的壁面反射模型示意图和刻蚀粒子数量分布。(a) 基于 micro-mask 的壁面反射模型示意图;(b) 不同基准高度的刻蚀粒子在水平方向上的数量分布

Fig. 8 Schematic of a wall reflection model based on micro-mask and distribution of etched particle quantity. (a) Schematic of a wall reflection model based on micro-mask; (b) quantity distribution of etching particles at different reference heights in the horizontal direction

整体来看,反射的刻蚀粒子的分布数量随水平方向距离的增大呈先增大再减小的趋势。根据刻蚀粒子聚集后的刻蚀效果,刻蚀粒子数量最大的位置为凹坑的最深处位置。随着基准高度 H 的增加,凹坑最深处的位置朝远离粒径中心的方向移动。当 micro-mask 的基准高度 H 为 $(1 \sim 5)R$ 时,刻蚀凹坑最深处的位置 $x_{de} \approx (2.5 \sim 6)R$ 。

为了验证 micro-mask 壁面反射增强模型,提出了以旋涂金纳米颗粒作为 micro-mask 的实验方法。首先将质量浓度为 0.005 mg/mL 的金纳米颗粒胶体溶液旋涂到样品表面,旋涂转速为 4000 r/min ,旋涂时间为 30 s 。图 9 为扫描电子显微镜下的金纳米颗粒图像。然后开展大气等离子体刻蚀实验,刻蚀参数如 2.2.2 节所示。

图 10 为原子力显微镜测量得到的表面带金纳米

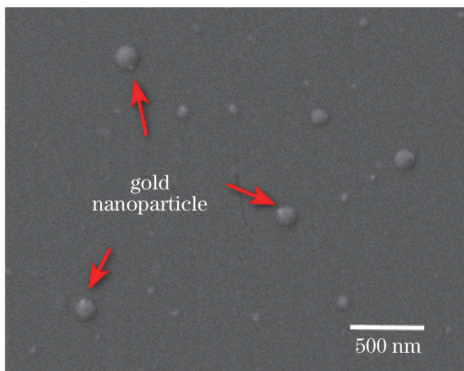


图 9 金纳米颗粒的扫描电子显微镜图像
Fig. 9 SEM image of gold nanoparticles

颗粒的样品经大气等离子体刻蚀后的表面形貌,其中右侧为左侧截线处样品表面轮廓的剖视曲线。由图 10 可以看出,经大气等离子体刻蚀后,元件表面上在金纳米颗粒的周围出现了凹坑。金纳米颗粒半径 R 约为 100 nm ,在原子力显微镜测量的样品表面形貌图上,分别选取金纳米颗粒中心位置和凹坑边缘位置,在右侧的剖视曲线上即得到凹坑边缘距金纳米颗粒中心的水平距离,约为 $0.94 \mu\text{m}$,即 $r_{di} \approx 9.4R$ 。基准高度 H 约为 $5R$,刻蚀凹坑最深处的位置距金纳米颗粒中心的水平距离约为 $0.65 \mu\text{m}$,即 $x_{de} \approx 6.5R$ 。图 10 中刻蚀凹坑最深处的位置和式(3)所示的理论模型完全吻合。通过上述金纳米颗粒的刻蚀实验结果,验证了 micro-mask 壁面反射增强模型的正确性,解释了大气等离子体刻蚀后元件表面凹坑的形成过程。

在大气等离子体刻蚀过程中,刻蚀反应生成的不挥发物会吸附并沉积于元件表面,形成 micro-mask,刻蚀粒子入射至 micro-mask 表面时发生壁面反射增强,在元件表面诱导形成凹坑微结构。为了改善大气等离子体刻蚀后元件表面的质量,可以采取一些工艺手段,例如增加氧气流量来抑制氟碳化合物的生成,或者使用氧化铈抛光或离子束抛光等技术进行处理,改善元件的表面形貌,拓展大气等离子体刻蚀的应用场景。

5 结 论

研究了抛光石英经过大气等离子体刻蚀后表面形貌的形成机理。首先开展了以大气等离子体刻蚀为前处理,再使用氢氟酸刻蚀的组合实验,证实了大气等离子体刻蚀后的熔石英元件表面不仅沉积有氟碳化合物,

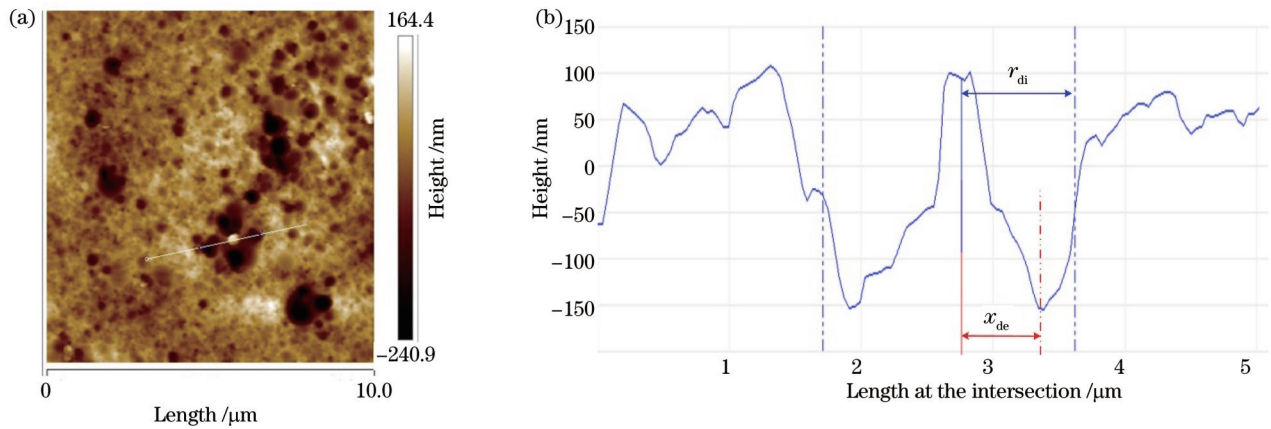


图 10 大气等离子体刻蚀下元件表面的金纳米颗粒的截面图

Fig. 10 Cross sectional view of gold nanoparticles on surface of the component under atmospheric plasma etching

还存在凹坑微结构。然后提出了基于 micro-mask 的壁面反射增强模型,通过旋涂金纳米颗粒作为 micro-mask 的刻蚀验证实验,验证了 micro-mask 壁面反射增强模型的正确性,解释了大气等离子体刻蚀抛光石英表面形貌的形成过程。研究成果有利于揭示大气等离子体刻蚀后抛光石英表面形貌的恶化机制,对认识和理解大气等离子体的刻蚀作用及界面演变机理具有指导意义。

参 考 文 献

- [1] Moody J D, Pollock B B, Sio H, et al. The magnetized indirect drive project on the national ignition facility[J]. *Journal of Fusion Energy*, 2022, 41(1): 7.
- [2] Atzeni S, Batani D, Danson C N, et al. An evaluation of sustainability and societal impact of high-power laser and fusion technologies: a case for a new European research infrastructure [J]. *High Power Laser Science and Engineering*, 2021, 9(4): e52.
- [3] Zhao Z X, Chen H, Zhang Z M, et al. High peak power femtosecond cylindrical vector beams generation in a chirped-pulse amplification laser system[J]. *Chinese Optics Letters*, 2022, 20(3): 031405.
- [4] Keidar M, Weltmann K D, Macheret S. Fundamentals and applications of atmospheric pressure plasmas[J]. *Journal of Applied Physics*, 2021, 130(8): 080401.
- [5] Sun R Y, Nozoe A, Nagahashi J, et al. Novel highly-efficient and dress-free polishing technique with plasma-assisted surface modification and dressing[J]. *Precision Engineering*, 2021, 72: 224-236.
- [6] Jin C Y, Wu W, Cao L, et al. Fabrication of lithium niobate metasurfaces via a combination of FIB and ICP-RIE[J]. *Chinese Optics Letters*, 2022, 20(11): 113602.
- [7] Gerhard C, Weihs T, Tasche D, et al. Atmospheric pressure plasma treatment of fused silica, related surface and near-surface effects and applications[J]. *Plasma Chemistry and Plasma Processing*, 2013, 33(5): 895-905.
- [8] 彭冰, 赖爱欢, 吴伦哲, 等. 大气等离子体变去除函数加工方法研究[J]. *中国激光*, 2021, 48(24): 2403002.
Peng B, Dun A H, Wu L Z, et al. Variable removal function in atmospheric pressure plasma polishing[J]. *Chinese Journal of Lasers*, 2021, 48(24): 2403002.
- [9] Lee S H, Lu J Q. Nano-ring-shape growth of fluorocarbon macromolecules during SiO₂ etching[J]. *Nanotechnology*, 2010, 21(15): 155303.
- [10] 李雨菡, 肖华攀, 王海容, 等. 湿法刻蚀处理熔石英光学元件研究进展[J]. *激光与光电子学进展*, 2021, 58(15): 1516026.
- [11] Li Y H, Xiao H P, Wang H R, et al. Review on wet etching technique of fused silica optical elements[J]. *Laser & Optoelectronics Progress*, 2021, 58(15): 1516026.
- [12] Martin M, Cunge G. Surface roughness generated by plasma etching processes of silicon[J]. *Journal of Vacuum Science & Technology B*, 2008, 26(4): 1281-1288.
- [13] Boulouis G, Constantoudis V, Kokkoris G, et al. Formation and metrology of dual scale nano-morphology on SF₆ plasma etched silicon surfaces[J]. *Nanotechnology*, 2008, 19(25): 255301.
- [14] 杨李茗, 黄进, 刘红婕, 等. 熔石英元件紫外脉冲激光辐照损伤特性研究进展综述[J]. *光学学报*, 2022, 42(17): 1714004.
Yang L M, Huang J, Liu H J, et al. Review on damage characteristics of fused silica elements irradiated by ultraviolet pulsed laser[J]. *Acta Optica Sinica*, 2022, 42(17): 1714004.
- [15] Jin H L, Xin Q, Li N, et al. The morphology and chemistry evolution of fused silica surface after Ar/CF₄ atmospheric pressure plasma processing[J]. *Applied Surface Science*, 2013, 286: 405-411.
- [16] Jin H L, Fan F, Yuan Z G, et al. Investigation of the formation mechanism of the fluorocarbon film in CF₄ plasma processing of fused silica[J]. *Optik*, 2020, 202: 163693.
- [17] Jiang X L, Wu L X, Yang K, et al. Kinetic etch front instability responsible for roughness formation in plasma etching[J]. *Applied Surface Science*, 2021, 543: 148862.
- [18] Jung S T, Song H S, Kim D S, et al. Inductively coupled plasma etching of Ge-doped boron-phosphosilicate glass for planar lightwave circuit devices[J]. *Journal of Non-Crystalline Solids*, 1999, 259(1/2/3): 191-197.
- [19] Choi D Y, Lee J H, Kim D S, et al. Formation of plasma induced surface damage in silica glass etching for optical waveguides[J]. *Journal of Applied Physics*, 2004, 95(12): 8400-8407.
- [20] Rad M A, Ibrahim K, Mohamed K. Formation of SiO₂ surface textures via CHF₃/Ar plasma etching process of poly methyl methacrylate self-formed masks[J]. *Vacuum*, 2014, 101: 67-70.
- [21] Zimin S P, Goralchev E S, Amirov I I, et al. Micromasking effect and nanostructure self-formation on the surface of lead chalcogenide epitaxial films on Si substrates during argon plasma treatment[J]. *Journal of Physics D: Applied Physics*, 2009, 42(16): 165205.
- [22] Li D, Li N, Su X, et al. Characterization of fused silica surface topography in capacitively coupled atmospheric pressure plasma processing[J]. *Applied Surface Science*, 2019, 489: 648-657.
- [23] Jiao P Q, Xin Q, Fan B, et al. Morphology evolution of Vickers

- indentation in fused silica glass etched by atmospheric pressure plasma jet[J]. *Ceramics International*, 2022, 48(21): 31500-31508.
- [23] Chen J, Cheng X, Wu L Z, et al. Research on competition evolution for increasing damage threshold of fused silica by atmospheric pressure plasma processing[J]. *Optical Engineering*, 2022, 61(6): 063101.
- [24] Suratwala T I, Miller P E, Bude J D, et al. HF-based etching processes for improving laser damage resistance of fused silica optical surfaces[J]. *Journal of the American Ceramic Society*, 2011, 94(2): 416-428.
- [25] Bosso P, Fanelli F, Fracassi F. Deposition of water-stable coatings containing carboxylic acid groups by atmospheric pressure cold plasma jet[J]. *Plasma Processes and Polymers*, 2016, 13(2): 217-226.

Research on Formation Mechanism of Fused Silica Etched Morphology Based on Wall Reflection Enhancement Model

Chen Jun^{1,2}, Wang Lin^{1*}, Wei Chaoyang¹, Shao Jianda¹

¹*Precision Optical Manufacturing and Testing Center, Shanghai Institute of Optics and Fine Mechanics, Chinese Academy of Sciences, Shanghai 201800, China;*

²*College of Materials Science and Opto-Electronic Technology, University of Chinese Academy of Sciences, Beijing 100049, China*

Abstract

Objective Fused silica has been widely applied in laser fusion devices due to its mechanical, optical, and thermal properties, such as diffractive elements, windows, shields, and other components. Atmospheric pressure plasma processing (APPP) is a non-contact material removal method based on a pure chemical reaction and features low cost and controllable material removal without contact and damage. It shows great potential for high-precision fabrication of fused silica optics. However, the material removal mechanism of pure chemical reaction will lead to the deteriorated surface morphology of fused silica processed by APPP, which seriously affects the performance and life of optics. It is necessary to reveal the formation mechanism of deteriorated surface morphology of fused silica to optimize the role of APPP in the optical surfacing.

Methods (1) Sample preparation. Fused silica samples (JGS1) provided by China Building Materials Academy are polished with traditional ceria oxide polishing. The diameter and thickness of fused silica samples are 50 mm and 5 mm respectively. All samples are deeply etched with hydrofluoric acid to remove the redeposition layer and subsurface damage. These samples are cleaned through multi-frequency ultrasonic with deionized water. The cleaning temperature is 45 °C and the ultrasonic frequency are 40, 75, and 120 kHz. The cleaning time of each frequency is 3 min. (2) Samples processed by atmospheric pressure plasma. These samples are etched by a capacitively coupled atmospheric pressure plasma. The experimental parameters are 170 W RF (radio frequency) power with 13.56 MHz frequency, 100 mL/min CF₄ (carbon tetrafluoride) as a reactive gas, 1800 mL/min He (helium) as a carrier gas, and 20 mL/min O₂ (oxygen) as auxiliary gas. The gap between the workpiece and electrode tip is 2 mm and the scanning speed of atmospheric pressure plasma is 60 mm/min. The point spacing and line spacing of discrete points in the circular grating path are 1 mm. (3) Samples processed by hydrofluoric acid. The samples etched by atmospheric pressure plasma are immersed in 20% mass fraction hydrofluoric acid for uniform etching. The hydrofluoric acid etching is carried out for 30 min in megasonic conditions (1 MHz). The removal depth of each side of the sample is about 5 μm.

Results and Discussions These fused silica samples are etched by atmospheric pressure plasma and then hydrofluoric acid to analyze the reasons for the deteriorated surface morphology. Compared with the untreated sample (roughness Ra of 0.56 nm), the results show that the surface morphology of fused silica etched by atmospheric pressure plasma becomes very rough (roughness Ra of 7.58 nm). The surface morphology of the sample is relatively flat (roughness Ra of 2.44 nm) after hydrofluoric acid etching. Additionally, the scanning electron microscope (SEM) pictures and X-ray photoelectron spectroscopy (XPS) results illustrate that the fluorocarbon appearing on the sample surface after plasma etching and the content of fluorine slightly decrease after hydrofluoric acid etching. This is because the fluorocarbon is generated and adsorbed on the sample surface during the atmospheric plasma etching. The deposition is effectively removed and the surface pits are merged after hydrofluoric acid etching. It is indicated that there is a fluorocarbon thin film and pits microstructure on the surface of fused silica etched by plasma. The formation mechanism of the pits microstructure on the

sample is inferred to be related to the particle deposits from the detailed information of the magnification pits picture. Then, a model based on the wall reflection enhancement is proposed to analyze the formation mechanism of surface pits microstructure on the sample in our paper. An etching experiment with spin-coated gold nanoparticles acting as a micro-mask on the surface is carried out to verify the model. The experimental results show that the position of the deepest part of the etching pit is inconsistent with the theoretical model. This confirms the correctness of the wall reflection enhancement model and explains the formation of pits microstructure on the sample surface after atmospheric plasma etching. The formation mechanism of pits microstructure during plasma etching is explained as follows. The non-volatile substances generated by the etching process can adsorb and deposit on the surface to form a micro-mask. The wall reflection enhancement occurs when etched particles are incident on the micro-mask surface to induce the formation of pit microstructures on the surface. Some measures, such as increasing the oxygen flow rate to suppress the fluorocarbon generation, can be taken to improve the surface morphology of fused silica etched by atmospheric plasma.

Conclusions The formation mechanism of fused silica etched morphology based on the wall reflection enhancement model is studied in our paper. It is confirmed that the deteriorated surface morphology of fused silica etched by plasma results from the deposition of fluorocarbon film and the pit microstructures on the surface through the hydrofluoric acid etching experiments. A wall reflection enhancement model based on the micro-mask is proposed. The experimental and simulated results verify the correctness of the wall reflection enhancement model. Finally, new ideas and methods are provided for solving the deteriorated surface morphology of fused silica etched by atmospheric pressure plasma.

Key words wall reflection enhancement; fused silica; surface morphology; formation mechanism; atmospheric plasma